Submitted to `FIXME: We don't submit papers to DIS...`

XIIIth International Workshop on Deep Inelastic Scattering, DIS 2005, April, 2005, Madison

Abstract: **xx-xxx**

Parallel Session **x**

www-h1.desy.de/h1/www/publications/conf/conf_list.html

Photoproduction of $D^{*\pm}$ Mesons Associated with a Jet at HERA

H1 Collaboration

Abstract

A measurement of cross sections for photoproduction of $D^{*\pm}$ mesons associated with a jet is presented. The data are taken with the H1 detector at HERA during the years 1999 and 2000. Photoproduction is selected by detecting the scattered electron at small angles. The cross sections are determined in the kinematic region $171 < W < 256$ GeV, $Q^2 < 0.01$ GeV^2, $p_t(D^*) > 2.0$ GeV and $|\eta(D^*)| < 1.5$, where W is the photon-proton centre-of-mass energy, Q^2 is the photon virtuality and p_t and η denote transverse momentum and pseudorapidity respectively. Jets are defined by the inclusive k_t algorithm. The jet with the highest transverse momentum $p_t(jet) > 3$ GeV that does not contain the D^* meson is taken. Differential cross sections are shown in $p_t(jet)$, $p_t(D^*)$, $\eta(jet)$, $\eta(D^*)$ and the azimuthal differences between the D^* and the jet, $\Delta\phi(D^*, \text{jet})$. The results are compared with QCD predictions in collinear and k_t-factorisation.

Version 2.4p (April 11, 2005)

1 Introduction

(Many more details can be found in Gero Flucke's thesis [1].)

The measurement of inclusive D^* production is interesting as a general test of the production mechanism. The measurements are consistent with the assumption that heavy quarks are predominantly produced via a boson gluon fusion mechanism, cf. figure 1.

The measurement of a D^*+jet pair gives the possibility to investigate further details of the charm production mechanism. The assumption is that the D^* meson and the jet approximate the kinematics of a charm or anti-charm quark and another parton, be it the other (anti-)charm, a light quark or a gluon.

Apart from single differential cross sections as a function of the transverse momenta and pseudorapidity of the D^* and the jet, measurements of observable of the D^*+jet system provide further stringent tests on the QCD calculations. The measurement of the difference in azimuthal angle $\Delta\phi(D^*, \text{jet})$ of the D^*+jet system are presented here. In a $2 \rightarrow 2$ process, $\Delta\phi(D^*, \text{jet})$ is exactly $180°$. Smaller $\Delta\phi(D^*, \text{jet})$ can be due to additional (gluon) radiation and/or due to intrinsic transverse momenta k_t of the partons initiating the heavy quark production process. The measurement of $d\sigma/d\Delta\phi(D^*, \text{jet})$ provides thus a crucial test of the QCD calculation and the treatment of higher order QCD contributions. An illustrating sketch of the different contributions to the $\Delta\phi(D^*, \text{jet})$ distribution are shown in figure 2.

2 Data Selection

Data of the years 1999 and 2000 with an integrated luminosity of $\mathcal{L} = 51.1$ pb^{-1} are analysed where protons of 920 GeV have been collided with positrons of 27.6 GeV. The data selection is similar to the preliminary inclusive D^* measurement [2]. Photoproduction is selected through the reconstruction of the scattered electron at small scattering angle $\pi - \theta_{e'} < 5$ mrad. This leads to the kinematic range of $Q^2 < 0.01$ GeV^2 and $0.29 < y < 0.65$. However, for the analysis presented here the transverse momentum cut for the D^* is lowered to $p_t(D^*) > 2.0$ GeV. The transverse momentum cut for the kaon is lowered to 0.3 GeV. This is possible due to

- the application of particle identification using dE/dx,
- a cut on the sum of the transverse momenta of the kaon and the pion from the D^0 decay, $p_t(K) + p_t(\pi) > 2.2$ GeV
- and the cut $p_t(D^*)/S_{E_t} > 0.10$, where S_{E_t} is the scalar sum of the all reconstructed hadronic final state (HFS) objects with polar angle $\theta > 10°$, $S_{E_t} = \sum_{HFS}^{\theta>10°} \sin\theta_i E_i$.

Details can be found in the chapters 4 and 5.1-3 of [1].

Jets are defined by the inclusive k_t-algorithm [3] in the p_t-recombination and ΔR-distance scheme. The input of the jet algorithm are hadronic-final-state objects (HFS) from combining tracks and clusters[1]. The algorithm is run in the laboratory frame. Since the algorithm is invariant under longitudinal Lorentz boosts, in photoproduction the result is the same as if the algorithm would be applied in the photon-proton centre-of-mass system.

To ensure that all decay particles of the D^* candidate end up in the same jet, the HFS objects of the D^* decay tracks are replaced by the D^* candidate itself, i. e. the four-vectors that belong to the D^* decay tracks are replaced by the sum of the momenta of the tracks assigning the kaon and pion mass respectively.

In events which contain more than one D^* candidate, the jet algorithm is run separately for each candidate. For each candidate only its own decay tracks are replaced by the D^* candidate.

The minimal required transverse momentum is $p_t(\text{jet}) > 3$ GeV. To ensure a satisfying transverse momentum measurement even at these low values of p_t, jets are restricted to the central detector region $|\eta(\text{jet})| < 1.5$ where well measured tracks dominate the HFS objects.

The aim is to tag a second object besides the D^* from the hard process. Therefore the jet not containing the D^* meson is selected. If more than one such jet is found, the jet with the highest transverse momentum is chosen.

Figure 3a) shows the multiplicity of the (non-D^*-) jets. For 588 ± 46 i. e. about 50% of the D^* mesons at least one jet is found.

More details are given in chapter 6.1 of [1].

3 Control Distributions

Pseudorapidity and transverse momentum distributions of the data are reasonably described by the simulations based on PYTHIA and CASCADE, cf. figure 4. Since CASCADE predicts transverse momentum distributions slightly harder than observed in the data, it is re-weighted according to an exponential fit to the transverse momentum of the D^* meson.

Transverse momentum resolution: Jets down to $p_t(\text{jet}) > 3$ GeV are reasonably measurable and the transverse momentum resolution is of similar size for low (< 5.5 GeV) and high (> 11 GeV) transverse momentum jets as shown in figure 5.

Purities and stabilities of the measured jet and D^*+jet quantities are shown in figure 6. They are defined as

$$P = \left.\frac{N_{gen}^{rec}}{N^{rec}}\right|_{bin}, \qquad (1)$$

$$S = \left.\frac{N_{gen}^{rec}}{N_{gen}}\right|_{bin}. \qquad (2)$$

P and S are calculated under the condition that both a generated D^* meson and a reconstructed D^* candidate are found within the visible range of the inclusive D^* measurement. The reconstructed candidate must lie in the signal region $143 < \Delta m < 148$ MeV and have the same charge as the generated D^* meson. Under these conditions[2]

[1]Track-cluster matching as in HADROO2 [4], version 2.6.5, except that only tracks from the central tracker are taken into account.

[2]This means that fluctuations in and out of the sample are taken into account.

N_{gen} is the number of generated D^*+jet combinations in a bin,

N^{rec} is the number of reconstructed D^* meson candidates associated with a reconstructed jet in a bin and

N_{gen}^{rec} is the number of reconstructed D^*+jet combinations in a bin with a generated D^*+jet combination in the same bin.

For all quantities purity and stability both are well above 50% (except for the lowest $\Delta\phi(D^*, \text{jet})$ where anyway hardly any events are measured), making a bin-by-bin correction possible.

4 QCD Calculations

The results will be compared with two leading order calculations supplemented with parton showers, PYTHIA 6.1 and the k_t-factorising CASCADE 1.2, as well as next-to-leading calculations in the massive (FMNR) and massless (ZMVFNS) scheme. In all calculations the charm mass is set to $m_c = 1.5$ GeV and all apply Peterson fragmentation.

For PYTHIA three different processes are generated separately and added afterwards: direct photon-gluon fusion, resolved processes with a light quark or a gluon from the photon and charm excitation processes where a charm quark from the photon enters the hard scatter. In the latter process the charm quark is treated as a massless parton like the light quarks whereas in the other processes the charm mass is accounted for in all steps of the calculation. Proton and photon density parameterisations CTEQ5L [5] and GRV-H LO [6] are used.

The main parameters of the (massless) ZMVFNS and (massive) FMNR calculations are listed in the following tables where m_t basically denotes the transverse mass $m_t = \sqrt{m_c^2 + p_{t,c}^2}$ ($m_t = \sqrt{m_c^2 + p_{t,D^*}^2}$ for ZMVFNS).

ZMVFNS	Fragmentation	μ_r	μ_f	p-PDF	γ-PDF
decreasing σ		$2 \cdot m_t$	$1.25 \cdot m_t$		
default	BKK O [8]	m_t	$2 \cdot m_t$	CTEQ5M [5]	GRV [6]
increasing σ		m_t	$4 \cdot m_t$		

FMNR	μ_r	μ_f	m_c [GeV]	ϵ_{pet}	p-PDF	γ-PDF
decreasing σ	$2 \cdot m_t$	m_t	1.7	0.042		
default	m_t	$2 \cdot m_t$	1.5	0.035	CTEQ5M [5]	GRV-G HO [6]
increasing σ	$0.5 \cdot m_t$	$4 \cdot m_t$	1.3	0.028		

The massless scheme is expected to work well [7] for $p_t \gg m_c$ which might not be always satisfied for the phase space considered here. On the other hand the massive scheme neglects terms $\propto \alpha_s \ln(p_t/m_c)$ and might not be accurate for high transverse momenta.

4.1 Uncertainties of QCD calculations

In the recent H1 publication measuring beauty cross sections using the semileptonic decay of B hadrons into muons [12] the uncertainties of the FMNR calculations are estimated by varying both scales simultaneously up or down and varying the heavy quark mass at the same time. Also in the calculation of charm cross sections using $D^*\mu$ correlations [13] both scales are varied simultaneously, but the effect of varying the heavy quark mass only is added in quadrature. But when varying both scales simultaneously in the same direction the effects on the cross section partially cancel. On the other hand for single bins the effect of varying μ_r (which in general leads to the largest effect) can be small due to the cancellation of contrary effects (especially in infrared sensitive regions). Thus the uncertainty of the cross section prediction of the FMNR calculation will be estimated as follows: For each calculated bin the maximal deviation up- and downward obtained by individually varying the renormalisation scale, the factorisation scale and the charm mass define the upper and lower bound of the prediction.

The uncertainty of the ZMVFNS calculation is estimated by considering the influence of varying the scales. For this massless calculation a usual way is to multiply the scales with a factor 2 or 0.5. The largest deviations from the central choice obtained by all combinations of variations define the lower and upper bound of the uncertainties. Mostly these are the diagonal scale variations, i. e. factor 2 for μ_r combined with factor 0.5 for μ_f and vice versa. The lowest minimal transverse momentum in this analysis, $p_t(D^*) = 2$ GeV, would lead to scales smaller than the starting scale Q_0 of the parton density parameterisations (MRST03 [10]). Therefore, the lowest scale used here is $\mu_f = 1.25 \cdot m_t$ compared to the central value of $\mu_f = 2 \cdot m_t$.

For the CASCADE calculations the renormalisation scale $\mu_r^2 = 4m_c^2 + p_t^2$ is chosen and the gluon density set A0 [14] is used. The importance of higher order terms is estimated by using the sets A0+ and A0- instead which apply the renormalisation scale multiplied and divided by two, respectively. Separately the charm mass has been varied from the default value $m_c = 1.5$ GeV to $m_c = 1.3$ and $m_c = 1.7$ GeV. The largest deviations of these four calculations from the default set define the upper and lower bound of the uncertainties of the CASCADE calculation. In most regions of phase space considered in this analysis the mass variations have the largest effect.

For PYTHIA no uncertainties are determined.

5 Cross Sections Determination

The bin averaged differential cross section in a variable Y is calculated according to

$$\frac{d\sigma_{vis}(ep \to e'D^*\text{+jet}X)}{dY} = \frac{N(D^*) \cdot (1-r)}{\Delta Y \cdot \mathcal{BR}(D^* \to K\pi\pi_s) \cdot \mathcal{L} \cdot \epsilon}. \tag{3}$$

ΔY stands for the width of the considered bin and $N(D^*)$ is the number of D^* mesons associated with a jet in this bin. The correction for reflections from other D^0 decays in the Δm distributions is denoted $(1-r) = 0.965$ [15, 16], $\mathcal{BR}(D^* \to K\pi\pi_s)$ is the branching ratio of the analysed D^* decay chain, $\mathcal{L} = 51.1$ pb^{-1} is the integrated luminosity after correction for trigger prescales and ϵ is the product of the efficiencies of the reconstruction, particle identification, triggering and the electron tagger acceptance,

$$\epsilon = \epsilon_{\rm L1} \cdot \epsilon_{\rm L4} \cdot \epsilon'_{rec} \cdot \epsilon_{\rm dEdx} \cdot \mathcal{A}_{\rm ET33}. \tag{4}$$

The efficiency trigger level, L1 $\epsilon_{\rm L1}$, is determined from the simulation and has been cross checked with data for the inclusive D^* sample (chapter 5.5.1 in [1]). It is around 95% for the D^*+jet measurement. The efficiencies of the trigger level L4, $\epsilon_{\rm L4} = 0.97$, and of the particle identification, $\epsilon_{\rm dEdx} = 0.98$, cuts are determined from data and applicable as global factors independent of the observed quantity. The electron tagger acceptance $\mathcal{A}_{\rm ET33}$ as a function of the considered quantities is determined from the Monte Carlo event generators applying the run- and inelasticity dependent acceptance function. It is about 40% with small variations. The reconstruction efficiency ϵ'_{rec} is determined from the simulation.[3] As bin-by-bin correction it corrects also for migrations and lies between 30% and 55%.

The systematic uncertainties arise from the determination of these correction factors and are summarised in the following table.

Source	$\boldsymbol{\sigma_{sys}}[\%]$
inclusive D^*	
L1	4
L4	4
ET33 acceptance	6
track efficiency	11
particle ID	2
$\mathcal{BR}(D^{*+} \to K^-\pi^+\pi_s^+)$	2.5
other D^0 decays	1.5
determination of $N(D^*)$	3
luminosity $\mathcal{L}$	1.5
D^*+jet	
model dependence	< 9 (< 6 except lowest $\Delta\phi$)
energy scale	1.5
total	$\sim 15 - 17$

Most of these uncertainties are determined from the inclusive D^* sample. (details in chapter 5.5-6 of [1]).

The uncertainty due to model dependence is evaluated by using CASCADE instead of PYTHIA in the determination of $\epsilon_{\rm L1}$, ϵ'_{rec} and $\mathcal{A}_{\rm ET33}$. The uncertainty is assigned half of the resulting cross section difference.

The uncertainty of the LAr energy scale is very small since about 60% of the transverse momentum of the jets is measured by tracks and about 30% using the electromagnetic energy scale.

[3] `h1sim/h1rec S33000.R90720`, `S33101.R90721`, `S32800.R90717` and `S32300.R90713`

6 Results

The D^*+jet cross section as a function of p_t(jet) and $p_t(D^*)$ are shown in figure 7 and compared with predictions of PYTHIA, CASCADE, FMNR and ZMVFNS. Both distributions are rapidly falling towards higher transverse momenta, however the slope of the distributions is slightly different: the D^* transverse momentum distribution falls slightly more rapidly towards larger transverse momenta than the one of the jet not containing the D^*. The $d\sigma/dp_t$ cross sections are reasonably well described by all QCD calculations.

Cross sections as a function of the pseudorapidity of the jet and the D^*, respectively, are shown in figure 8. They differ noticeably: The $\eta(D^*)$ distribution falls steeply with increasing values of η (similar to the inclusive analysis) whereas η(jet) is almost flat. It has been checked that this difference is not caused by the slightly different kinematic cuts for the D^* and the jet, as can be seen from the direct PYTHIA distribution. The comparison of the $\eta(D^*)$ with the η(jet) cross sections suggests, that the jet cross section contains not only a charm jet in which case the D^* and the jet distributions would be expected to be similar. If, however, the jet cross section contains also contributions from hard gluon radiation from the initial state (such as included in a $\gamma g \to c\bar{c}g$ process), which tend to populate mainly the forward (large η) region, the behaviour of the measured cross section could be understood. This hypothesis is also supported from comparison with the QCD calculations, which show exactly this effect. For direct photon processes ($\gamma g \to c\bar{c}$) as simulated in PYTHIA dir, the η spectrum is found to be similar (figure 8 left), only after inclusion of the charm excitation processes, which effectively simulate processes like $\gamma g \to c\bar{c}g$, the η spectrum of the jet can be appropriately described. A similar feature is obtained with k_t factorisation as implemented in CASCADE, but also with the fixed NLO calculations.

The figure 10 presents the cross sections in bins of $\Delta\phi(D^*,\text{jet})$. It is interesting to observe, that only $\sim 25\%$ of the measured cross section come from a back to back configuration. Such a configuration would be observed if the dominant process would be $\gamma g \to c\bar{c}$. However the data suggest a large contribution of $\sim 75\%$ of higher order QCD radiation. In the DGLAP type event generator such contribution is simulated with the help of leading log parton showers, but also coming from the resolved photon processes and charm excitation. In the CASCADE calculation the $\Delta\phi(D^*,\text{jet})$ distribution is directly correlated with the k_t of the gluon generating the $c\bar{c}$ pair and therefore sensitive to the un-integrated gluon density.

In the NLO calculations $\Delta\phi(D^*,\text{jet}) \neq 180^o$ comes entirely from real gluon emission, and therefore the calculations are essentially LO for this observable. It is interesting to mention, that due to infrared sensitivity of the NLO calculations (FMNR and ZMVFNS) give a huge negative cross section in the highest $\Delta\phi(D^*,\text{jet})$ bin which is compensated by a large positive contribution in the next lower $\Delta\phi(D^*,\text{jet})$ bin, therefore both bins are averaged to be compared to the measurement. It is also interesting to observe, that the smaller $\Delta\phi(D^*,\text{jet})$ region is not described by the FMNR or ZMVFNS calculations indicating the sensitivity to even higher order contributions. It is still open, whether a calculation of $\mathcal{O}(\alpha_s^3)$ is sufficient to describe the measurement or whether a re-summation to all orders is needed.

Since PYTHIA predicts a contribution in the region $\Delta\phi(D^*,\text{jet}) \approx 100^\circ$ solely via resolved processes, it is unlikely that the missing cross section prediction of the NLO calculations in this region is caused by neglecting a transverse smearing in the D^* fragmentation of charm quark into the D^* meson.

6.1 ZMVFNS with other parton densities

The ZMVFNS calculations originally have been performed using the MRST03 (AFG04) parton densities for the proton (photon) [17]. But since MRST03 is fitted only in the region with $x > 0.005$ and scale $Q^2 > 10$ GeV^2 it is not appropriate for D^* production with low transverse momenta like in this analysis, cf. figure 11. Therefore the author of the calculations (Gudrun Heinrich) agreed to perform calculations using CTEQ5M. To be consistent with the FMNR calculations the new calculation uses GRV for the photon instead of AFG04.

For reference the figures 12, 13 and 14 show ZMVFNS calculations with different sets of parton densities. The influence of the photon density on the presented distributions is negligible whereas CTEQ5M leads to significantly higher predictions than MRST03, specifically where contributions from lower x_g are expected. The difference between CTEQ5M and CTEQ6M [9] (not shown) is negligable.

7 Conclusions

Photoproduction of D^* mesons has been analysed at relatively low transverse momenta. Cross sections have been determined for events that contain a D^* meson and a jet not containing the D^*. The results have been compared with four approaches of QCD calculations.

The measured transverse momentum distributions of the D^* and jet are in general in agreement with the prediction within the theoretical uncertainties.

Comparing the pseudorapidity distributions of the D^* and the jet it is striking that the $\eta(D^*)$ falls in forward direction whereas $\eta(\text{jet})$ is almost constant. This observation suggests that the jet cross section contains not only a charm jet but also a significant contribution form a further parton, most likely a gluon jet. The gluon radiation can be described by several approaches: By parton showers in combination with charm excitation processes (PYTHIA), an initial gluon ladder in k_t factorisation with a final state parton shower (CASCADE) or the presence of a gluon radiation in the hard process (NLO calculations).

The azimuthal difference $\Delta\phi(D^*, \text{jet})$ is sensitive to the amount of gluon radiation. The measured cross section shows, that only $\sim 25\%$ come from a LO process ($\gamma g \to c\bar{c}$) with a collinear gluon. The higher orders contribute significantly. The $\Delta\phi(D^*, \text{jet})$ is reasonably well described by calculations applying leading log parton showers in the collinear factorisation ansatz, or by using un-integrated gluon densities in the k_t-factorisation ansatz. It is interesting to observe, that the smaller $\Delta\phi(D^*, \text{jet})$ region is not described by the FMNR or ZMVFNS calculations indicating the sensitivity to even higher order contributions. It is still open, whether a calculation of $\mathcal{O}(\alpha_s^3)$ is sufficient to describe the measurement or whether a re-summation to all orders is needed.

References

[1] Photoproduction of D^* Mesons and D^* Mesons Associated with Jets at HERA, Gero Flucke, Universität Hamburg (2005), `DESY-THESIS-2005-006` (available as H1-thesis 380).

[2] `H1prelim-03-071`.

[3] S. Ellis, D. Soper, Phys. Rev., **D48**, (1993) 3160. `hep-ph/9305266`.

[4] An energy flow algorithm for Hadronic Reconstruction in OO: Hadroo2, H1 internal note (2005). `H1-01/05-616`

[5] H. L. Lai, *et al.* (CTEQ), Eur. Phys. J., **C12**, (2000) 375. `hep-ph/9903282`.

[6] M. Glück, E. Reya, A. Vogt, Phys. Rev., **D46**, (1992) 1973.

[7] W.-K. Tung, S. Kretzer, C. Schmidt, J. Phys., **G28**, (2002) 983. `hep-ph/0110247`.

[8] J. Binnewies, B. A. Kniehl, G. Kramer, Phys. Rev., **D58**, (1998) 014014. `hep-ph/9712482`.

[9] J. Pumplin, *et al.* (CTEQ), JHEP, **07**, (2002) 012. `hep-ph/0201195`.

[10] A. D. Martin, R. G. Roberts, W. J. Stirling, R. S. Thorne, in *XI International Workshop on Deep Inelastic Scattering (DIS 2003)* (eds. V. T. Kim, L. N. Lipatov), 150–154 (PNPI, 2003). `hep-ph/0307262`.

[11] P. Aurenche, J. P. Guillet, M. Fontannaz, *New NLO Parameterisations of the Parton Distributions in Real Photons* (2004/5). `hep-ph/0503259`.

[12] A. Aktas, *et al.* (H1), *To be submitted to* Eur. Phys. J., **C**. `DESY 05-004`. `FIXME: Is already published!`

[13] A. Aktas, *et al.* (H1), *Measurement of Charm and Beauty Photoproduction at HERA using $D^*\mu$ Correlations*, to be published (2005). `FIXME: Already published, at least hep-ex!`

[14] H. Jung, in *XII International Workshop on Deep Inelastic Scattering (DIS 2004)* (eds. D. Bruncko, J. Ferencei, P. Stríženec), vol. 1, 299–302 (SAS, 2004). `hep-ph/0411287`.

[15] C. Adloff, *et al.* (H1), Nucl. Phys., **B545**, (1999) 21. `hep-ex/9812023`.

[16] S. Hengstmann, *A Measurement of Diffractive Charm Production at HERA*, Ph.D. thesis, Universität Zürich (2000).

[17] G. Heinrich, B. A. Kniehl, Phys. Rev., **D70**, (2004) 094035. `hep-ph/0409303`.

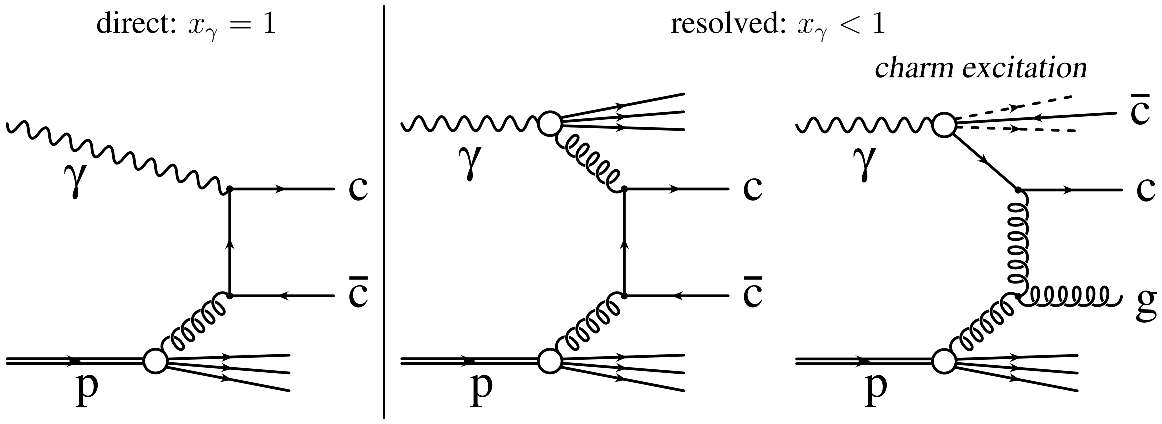

Figure 1: *The main charm production mechanisms in leading order photoproduction: direct and resolved where the latter are dominated by charm excitation in the photon.*

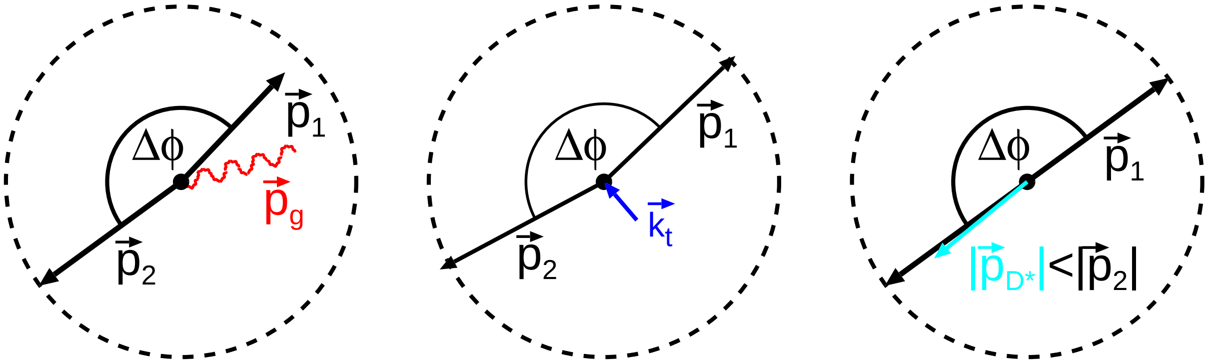

Figure 2: *Radial view illustrating how (gluon) radiation, incoming transverse momentum* k_t *or the fragmentation of the charm quark can lead to* $\Delta\phi(D^*, jet) < 180°$ *and* $p_t(D^*{+}jet) > 0$.

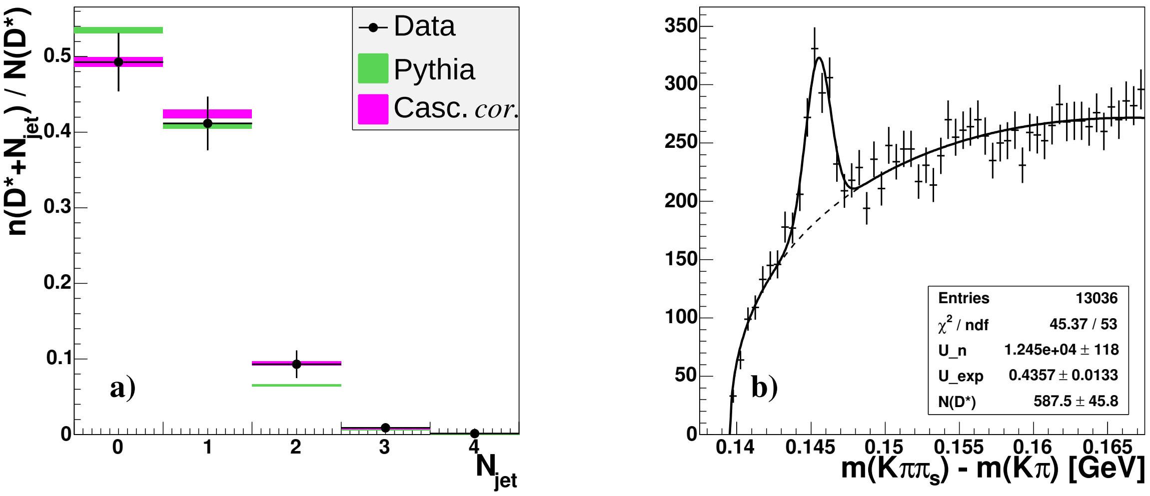

Figure 3: *Normalised number of reconstructed jets not containing the D^* meson (a) and Δm distribution of D^* mesons associated with at least one jet (b).*

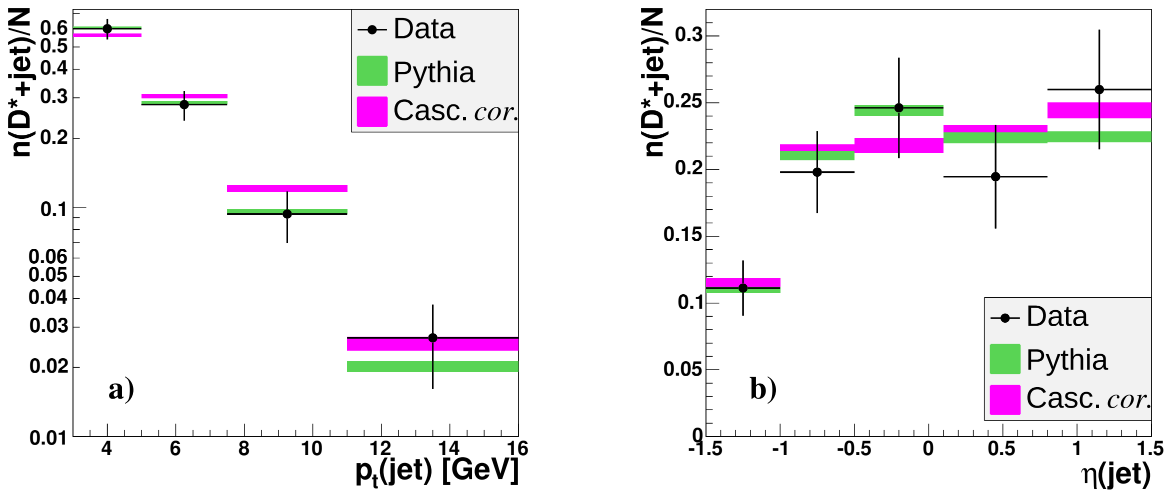

Figure 4: *Comparison of the normalised distributions of p_t (a) and η (b) of the selected jets in the data with the simulations PYTHIA and CASCADE. The CASCADE distribution is slightly re-weighted according to the generated $p_t(D^*)$.*

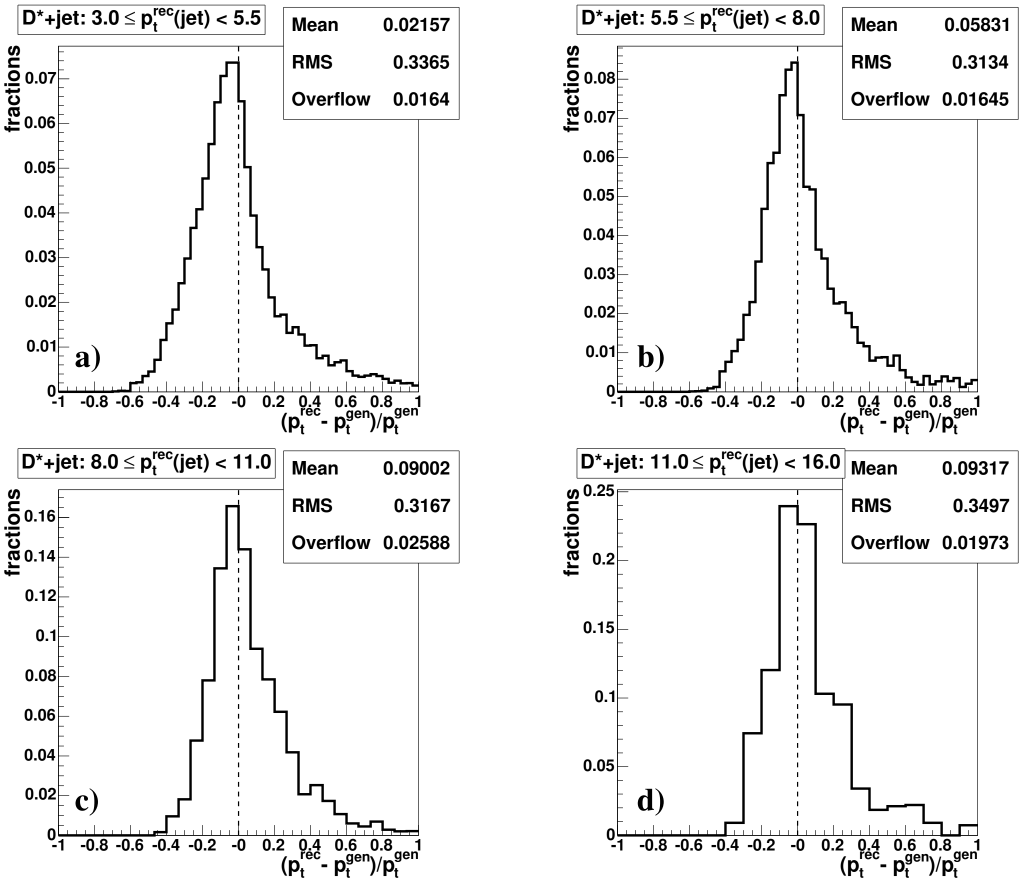

Figure 5: *Resolution of the transverse momentum measurement of the jet in bins of* $p_t^{rec}(jet)$. *All distributions are normalised to one.*

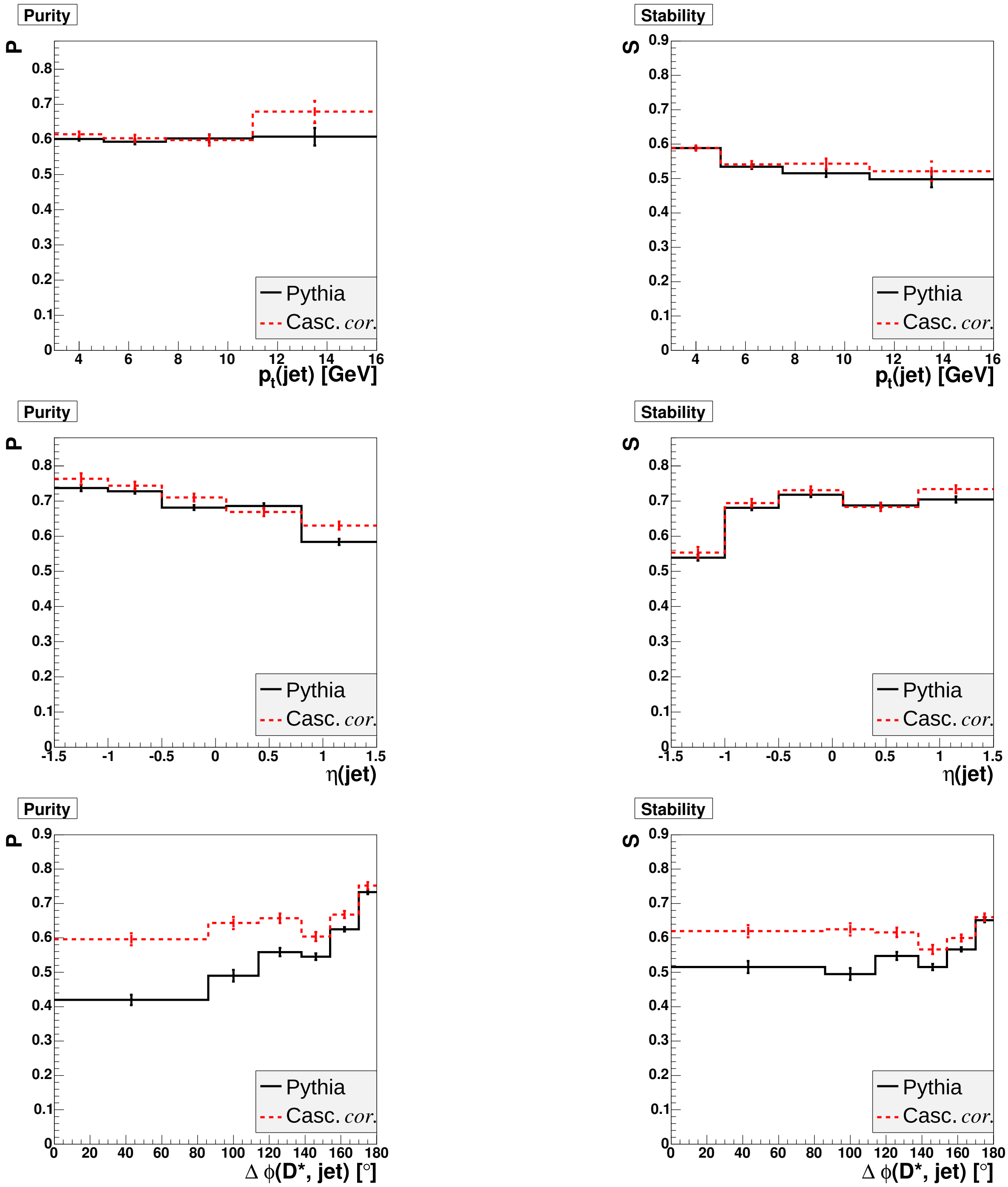

Figure 6: *Purity and stability in bins of the transverse momentum and the pseudorapidity of the jets and of the azimuthal difference between the* D^* *and the jet,* $\Delta\phi(D^*, jet)$.

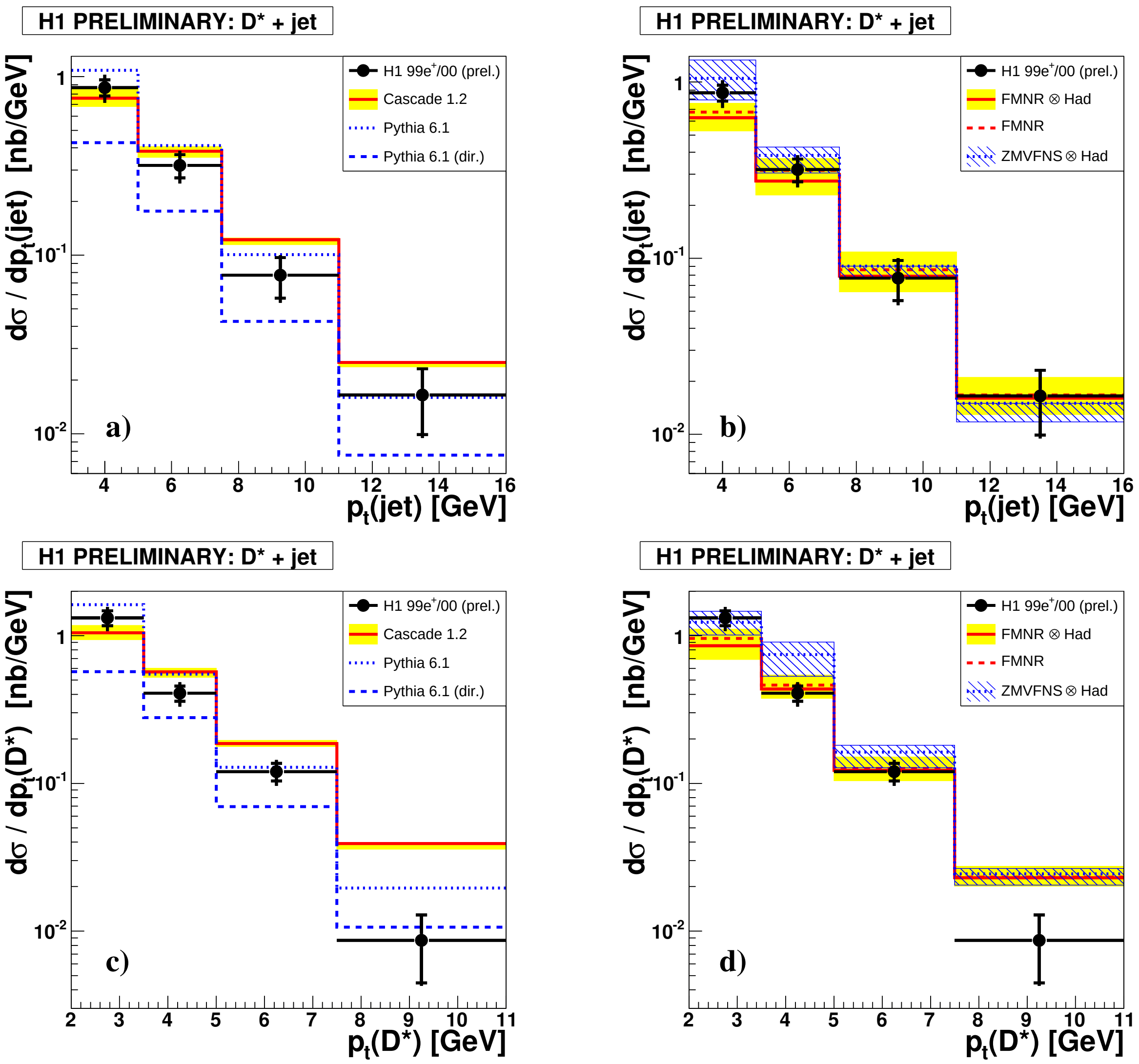

Figure 7: *D^*+jet cross sections in bins of the transverse momentum of the jet and the D^* compared with the predictions of PYTHIA and CASCADE (a,c) and of next-to-leading order calculations (b,d). FMNR is a* massive *and ZMVFNS a* massless *calculation. For PYTHIA the direct contribution of the prediction is shown separately and labelled as* "dir.". ***Plots aimed for preliminary.***

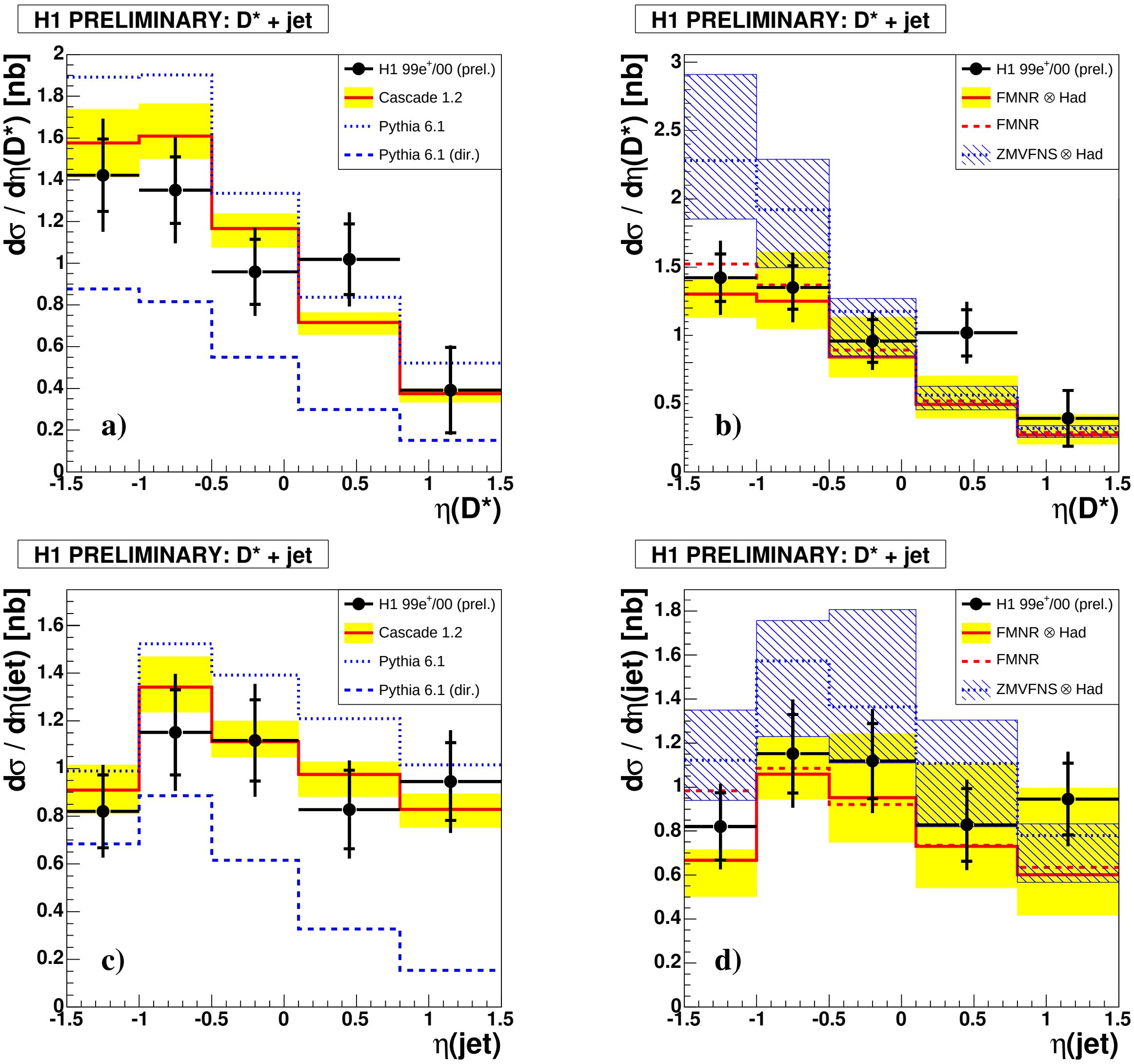

Figure 8: *D^*+jet cross sections in bins of $\eta(D^*)$ (a,b) and $\eta(jet)$ (c,d) compared with the predictions of PYTHIA and CASCADE on the left and of next-to-leading order calculations on the right. FMNR is a* massive *and ZMVFNS a* massless *calculation. For PYTHIA the direct contribution of the prediction is shown separately and labelled as* "dir.". ***Plots aimed for preliminary.***

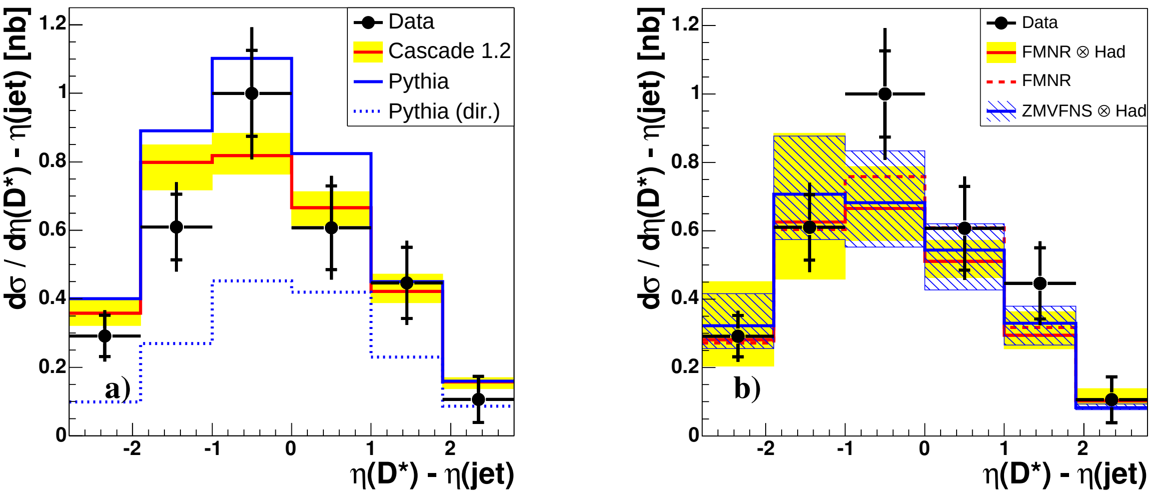

Figure 9: *Supporting figure: D^*+jet cross sections in bins of $\eta(D^*) - \eta(jet)$. (ZMVFNS with MRST03 (AFG04) for the proton (photon) parton densities.)*

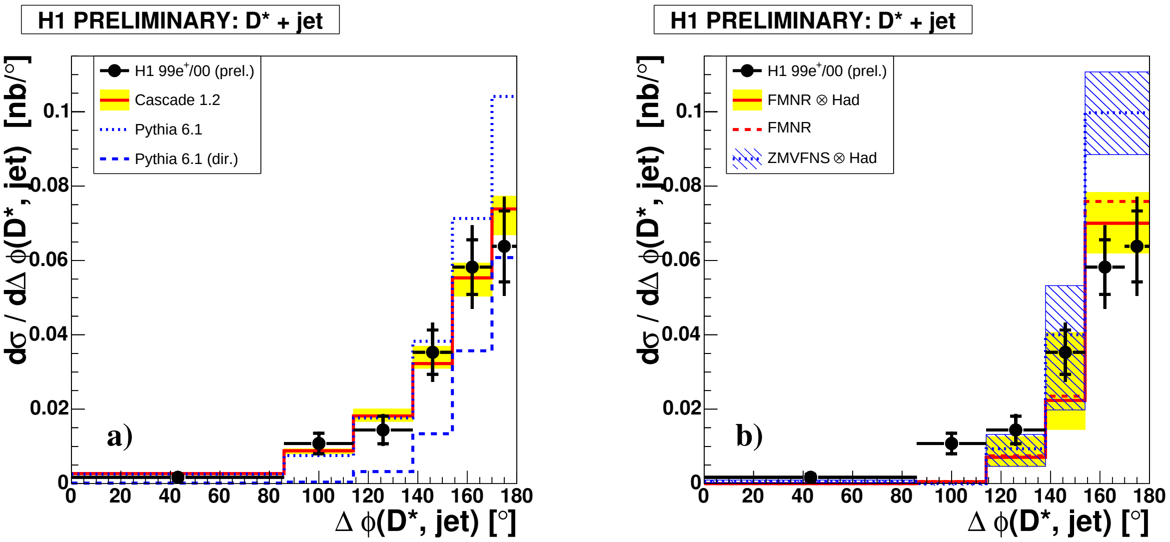

Figure 10: *D^*+jet cross sections in bins of $\Delta\phi(D^*, jet)$ compared with the predictions of PYTHIA and CASCADE on the left and of next-to-leading order calculations on the right. FMNR is a* massive *and ZMVFNS a* massless *calculation. For PYTHIA the direct contribution of the prediction is shown separately and labelled as* "dir.". ***Plots aimed for preliminary.***

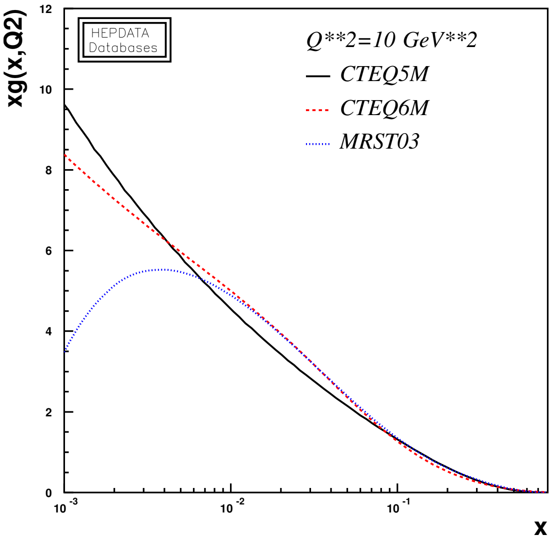

Figure 11: *Gluon densities at NLO at a scale* $\mu_f^2 = 10\ \mathrm{GeV}^2$. *The CTEQ5M [5] parameterisation is used for the (massive) FMNR and the (massless) ZMVFNS calculations. The MRST03 [10] parameterisation has also been used for the ZMVFNS and shows significant differences. But since it is fitted in a region with* $x > 0.005$ *and* $Q^2 > 10$ *GeV*^{2}*, it is not appropriate for charm photoproduction at HERA with low transverse momenta.*

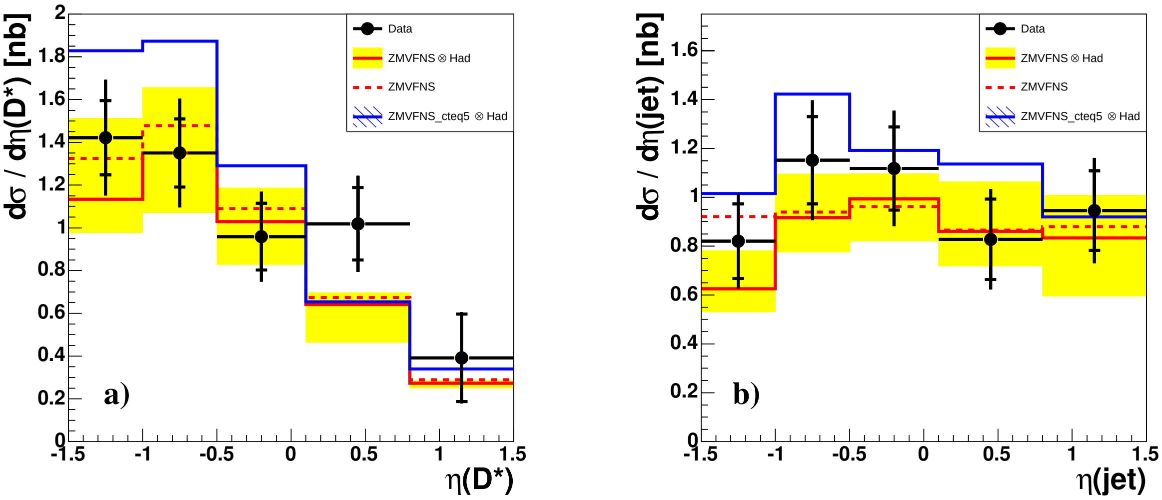

Figure 12: *Comparison of the ZMVFNS calculations using the MRST03 (default) and CTEQ5M parameterisation of the parton densities in the proton together with the data. In all regions where smaller* x_g *are expected to contribute CTEQ5M leads to higher cross section predictions as expected from figure 11. (AFG04 as photon density.)*

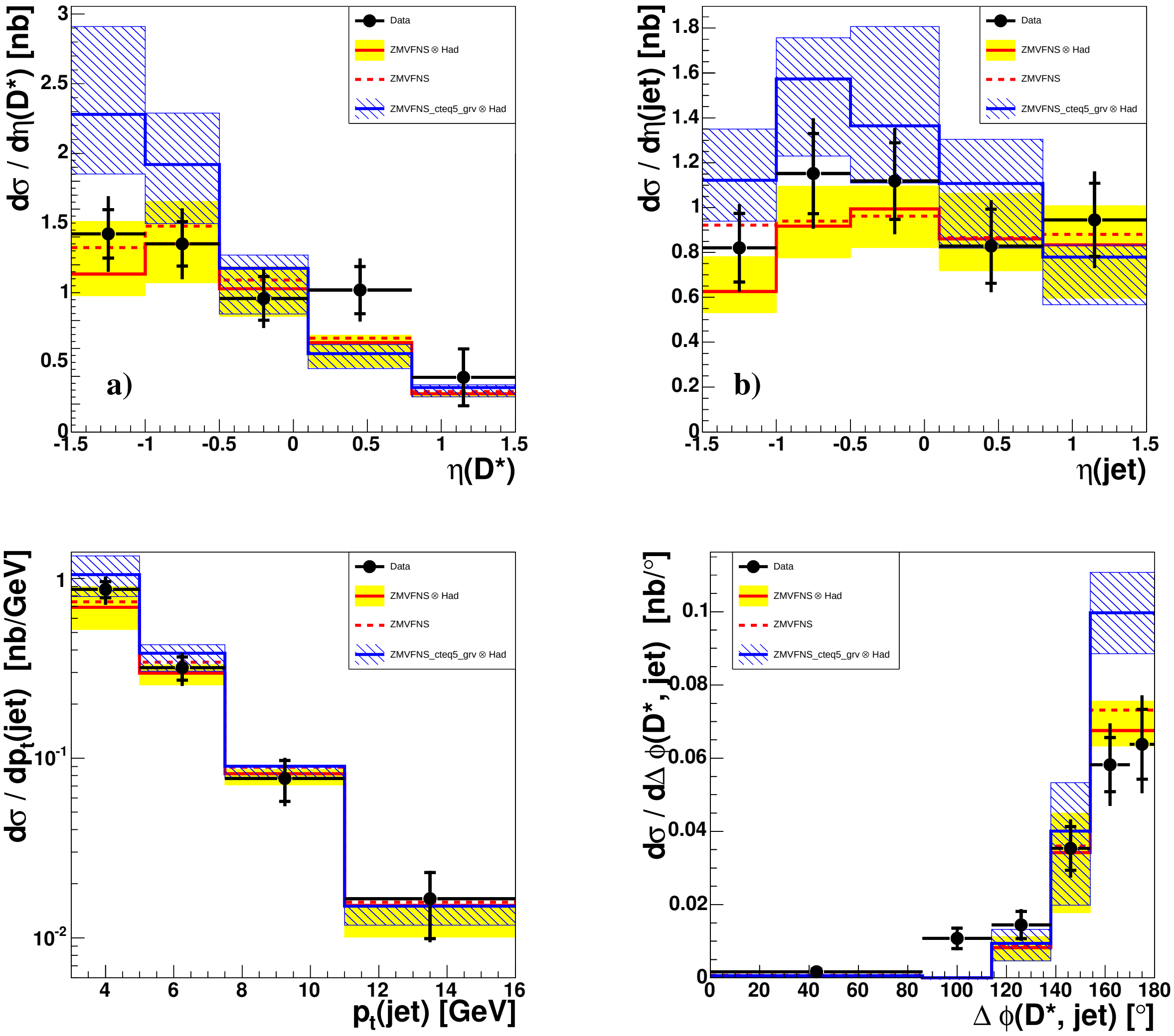

Figure 13: *ZMVFNS calculations using the MRST03c (AFG04) parameterisations of the parton densities in the proton (photon) and using CTEQ5M (GRV) compared to the data.*

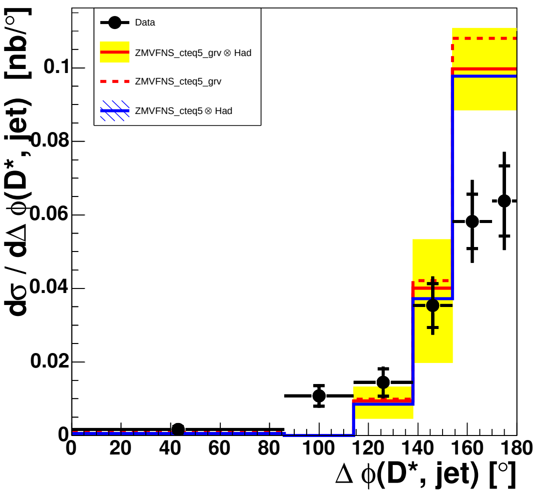

Figure 14: *ZMVFNS with CTEQ5M for the proton, but AFG04 or GRV for the photon.*